

Analyzing Achievable Stiffness Control Bounds of Robotic Hands With Coupled Finger Joints

Prashant Rao, Gray C. Thomas, Luis Sentis and Ashish D. Deshpande

Abstract—The mechanical design of robotic hands has been converging towards low-inertia, tendon-driven strategies. As tendon driven robotic fingers are serial chain systems, routing strategies with compliant tendons lead to multi-articular coupling between the degrees of freedom. We propose a generalized analysis of such serial chain linkages with coupled passive joint stiffnesses. We analyze the effect of such coupling on maximum achievable stiffness control boundaries while maintaining passivity at the actuators by analytically deriving the boundaries. We believe that we can use this information to form mechanical design guidelines for intelligently selecting arrangements of compliance elements (mechanical springs) and transmission strategies, i.e. tendon routing and pulley radii, to provide intrinsic stability and customizable controller stiffness limits for high performance manipulation in robotic hands.

I. INTRODUCTION

In the past decade, mechanical design of robotic hands [1] has moved away from large, rigid, direct-drive strategies [2] towards low inertia, tendon-driven actuation and passively compliant design [3], [4], [5]. Compliance is a key requirement for safe robotic interaction with the environment, and is actively implemented in robotic hands using impedance control strategies [6], [7], [8]. Impedance control laws require accurate knowledge of the manipulator's states and end-tip forces. Factors such as sensor noise, non-collocation of sensors and actuators, and feedback delays can make such controllers unreliable and introduce instability. Passive mechanical compliance in robotic systems can be used to augment the software control and it also offers many advantages over rigid robots, such as instantaneous response, decoupling of joints from actuator dynamics, compliance for safe interaction etc. [9], [10]. We are interested in making improvements to the mechanical design of multi-degree of freedom (DOF) robotic hands which incorporate springs, arranged in series and parallel with respect to the actuators, for high performance manipulation.

In robotic joints, we classify springs coupling actuators to joints as *series* compliance and springs coupling joints to actuator ground or other joints as *parallel* compliance. Series compliance in robotic joints has been extensively implemented [11], [12], [13] and its effects on compliance control previously studied [9], [14]. Parallel compliance has been implemented in legged robots for energy storing [15] and in robotic fingers to overcome under-actuation [5], [16]. A recent study [17] has shown that adding parallel

This work was supported in part by NASA (grant NNX15AQ33H) and also, in part, by the National Science Foundation (grant number 1157954). All authors are with the Department of Mechanical Engineering, The University of Texas at Austin, USA. Send correspondence to prashant.rao@utexas.edu

compliance to low-inertia, direct-drive robotic finger joints improves robustness and disturbance-rejection in presence of sensor noise and controller time delays. For stiffness-controlled robotic arms with independent series elasticity at every joint, it was shown that the controller stiffness at the joint can never exceed the stiffness of the series spring element at the joint [18]. Another study used series springs in the tendons of a 1-DOF robotic finger [14] and found that series compliance imposes a stability bound on the maximum feasible control stiffness, and that adding parallel compliance to such systems can increase the stable bounds on stiffness control. Both of these studies, however, apply to multi-DOF systems only in case of decoupled, independent joint stiffnesses. Other researchers have worked towards finding stable limits for Cartesian stiffness in multi-DOF compliant robots [19], [20] while assuming decoupled joint articulation.

Tendon driven fingers are serial chain manipulators whose joints will be inherently passively coupled for virtually every practical tendon routing strategy. Humans have similar passive coupling in their joints due to multi-articular muscles and tendons, and are able to exploit it to perform graceful manipulation and achieve stiffness control over their entire Cartesian workspace [21]. However, the effects and limitations of such passive mechanical coupling on stiffness-controlled robotic fingers have not been fully analyzed to date. In this paper we present a passivity-based analysis for low-inertia, series-elastic tendon-driven robotic fingers implementing stiffness control in joint space. We use this analysis to observe and understand the effect of the design parameters such as moment arms (pulley radii), parallel compliance and series compliance. We then validate the passivity bounds from our analysis on a two DOF tendon-driven robotic finger in both simulation and experiments. Our analysis leads to a design paradigm for optimizing the mechanical design parameters of the hands in order to allow robust, passive controllers to perform the desired manipulation skills.

II. SYSTEM MODELING

A. Basic Model

The following analysis presents a simple, linearized model of a generalized tendon-driven multi-DOF finger. The model assumes that there are m motors pulling on m cables, and that these cables have linear springs in series. The n joints of the robot hand are actuated by $m > n$ tendons arranged such that the tendon-map R has full column rank for controllability [22]. The transpose of the R matrix maps

TABLE I: Variables used in the model

n	$\in \mathbb{Z}, n > 0$	independent degrees of freedom
m	$\in \mathbb{Z}, m > n$	motor–tendons pairs
q	$\in \mathcal{Q} = \mathbb{R}^n$	joint angles
τ	$\in \mathcal{T} = \mathbb{R}^n$	joint torques.
K_d	$\in \mathbb{R}^{n \times n}$	desired stiffness matrix (diagonal)
R	$\in \mathbb{R}^{m \times n}$	tendon routing Jacobian (an injection)
K_s	$\in \mathbb{R}^{m \times m}$	tendon compliance. (diagonal, p.d.)
R_m	$\in \mathbb{R}^{m \times m}$	motor pulley radii (a bijection)
θ	$\in \Theta = \mathbb{R}^m$	motor angle
γ	$\in \Gamma = \mathbb{R}^m$	motor torque
γ'	$\in \Gamma' = R_m^T K_s R Q$	output-mapped motor torques
θ'	$\in \Theta' = R_m^{-1} R Q$	output-mapped motor angles

tendon tensions surjectively onto joint torques—many combinations of tendon forces produce the same torque vector. The tension force is based on the spring deflection which is the difference between motor side tendon displacement and joint side tendon displacement. The motor torque γ and joint torque τ are

$$\gamma = R_m^T (K_s (R_m \theta - R q)) \quad (1)$$

$$\tau = R^T (K_s (R_m \theta - R q)) \quad (2)$$

B. Output-Mapped Subspaces

Our stability analysis is based on the concept of passivity. If the motors are not adding energy to the mechanical system, then the system is bound to settle out eventually. In order to check this condition we analyze the controller as if it only had sensors at the motor–tendon interface—motor position and motor torque. The various equalities allow us to write all variables in the system in terms of motor interface variables. However, we need to keep in mind that only linear subspaces of motor interface variables actually move the hand—the output mapped subspace of motor torque Γ' and the output mapped subspace of motor angle Θ' . The rest of the system doesn't influence the hand's motion, doesn't interact with the unknown environment, and therefore doesn't need to be held to the passivity criterion.

All possible joint torque vectors can be accomplished by moving the motor positions, but many different motor position vectors may produce the same joint torque vector. The set of all motor position vectors that produce the same joint torque vector, set Θ_τ for torque τ , can be characterized by a representative motor position vector and the null space $N[R^T K_s R_m]$ of the $R^T K_s R_m$ operator.

$$\Theta_\tau = \{\theta : R^T K_s R_m \theta = \tau\} \quad (3)$$

$$= \{R_m^{-1} K_s^{-1} B R (R^T B R)^{-1} \tau + n : n \in N[R^T K_s R_m]\} \quad (4)$$

where B is a dummy variable which selects a representative subset of dimension n so long as $R^T B R$ is invertible.

A logical choice here is $B = K_s$. In this case the set of representatives,

$$\Theta' = \{\theta' : \theta' = R_m^{-1} R (R^T K_s R)^{-1} \tau, \tau \in \mathcal{T}\}, \quad (5)$$

is equivalent to the space defined by the image of \mathcal{Q} under $R_m^{-1} R$. This type of output-mapped subspace also exists

for Γ , the space of motor torques, as shown in Tab. II. Ultimately we will ignore the non-output-mapped portion of these spaces and focus our attention on a feedback controller acting in the output-mapped space. To implement such a controller in a practical tendon driven system, a variable from the null-space $\theta_t \in N[R^T K_s R_m]$ must be chosen to define the complete motor angle vector $\theta = \theta_t + \theta'$. This should be chosen such that the total tendon force vector $K_s (R_m \theta' + R_m \theta_t - R q)$ has only positive tensions¹. In belt-driven systems, mechanical pre-tension can substitute θ_t .

C. Desired Position

The goal of our controller is to enact a desired stiffness law by measuring joint position and setting a position control set point, θ_d , for the pulley motors. We will use (2) to find this (output-mapped) $\theta_d \in \Theta'$ to enforce the stiffness law $\tau = -K_d q$:

$$[R^T K_s R - K_d] q = R^T K_s R_m \theta_d, \quad \theta_d \in \Theta'. \quad (6)$$

where K_d is a diagonal matrix of desired independent joint stiffnesses.

We name this bracketed matrix the effective controller stiffness matrix (\mathbf{K}_c)

$$\mathbf{K}_c := R^T K_s R - K_d. \quad (7)$$

The effective controller stiffness matrix describes a force generating system $\tau = \mathbf{K}_c q$ which, if placed in parallel with the joints of the finger, would counterbalance the series stiffness and bring about the desired behavior. To further understand the characteristics of this matrix, we proceed to represent this same controller as if it acted at the motor interface.

We return to our expression (1) for γ , and restrict our attention to the output-mapped motor variables by pre-multiplying with the projector matrix $R_m^T K_s R (R^T R)^{-1} R^T K_s^{-1} R_m^{-T}$ (from table II, $\Gamma \rightarrow \mathcal{Q} \rightarrow \Gamma'$),

$$\gamma' = R_m^T K_s R_m \theta' - R_m^T K_s R q, \quad (8)$$

With (8) we can use motor interface variables to compute the joint angles. First, we pre-multiply by $(R^T R)^{-1} R^T K_s^{-1} R_m^{-T}$ (also from table II, $\Gamma \rightarrow \mathcal{Q}$)

$$q = (R^T R)^{-1} R^T R_m \theta' - (R^T R)^{-1} R^T K_s^{-1} R_m^{-T} \gamma' \quad (9)$$

To keep the algebra manageable, we define

$$K_m := R_m^T K_s R_m, \quad (10)$$

$$A := (R^T R)^{-1} R^T K_s^{-1} R_m^{-T}, \quad (11)$$

and simplify:

$$q = A K_m \theta' - A \gamma'. \quad (12)$$

Returning to (6), substituting (12), and pre-multiplying by A^T ,

$$A^T \mathbf{K}_c A K_m \theta' - A^T \mathbf{K}_c A \gamma' = \theta_d \quad (13)$$

¹In tendon driven fingers with non-linear stiffness, θ_t could be actively controlled to alter the pre-tension in all the tensions and thus influence the linearized stiffness K_s .

TABLE II: Output-Mapped Subspaces

space	forward map from $\mathcal{Q} \mapsto$ this space	inverse map from this space $\mapsto \mathcal{Q}$
\mathcal{Q} – space of joint angles	I	I
\mathcal{T} – space of joint torques	$R^T K_s R$	$(R^T K_s R)^{-1}$
Γ' – output mapped subspace of motor torques	$R_m^T K_s R$	$(R^T R)^{-1} R^T K_s^{-1} R_m^{-T}$
Θ' – output mapped subspace of motor angles	$R_m^{-1} R$	$(R^T R)^{-1} R^T R_m$

And in this final form we have our control, θ_d , as a function of output-mapped motor interface variables.

D. Including motor dynamics

We ignore the non output-mapped subspace and assume that the actuator position controllers have been tuned so that they behave like first order systems with one time constant (p) for all motors.

$$\dot{\theta}' = pI(\theta_d - \theta'), \quad p > 0 \quad (14)$$

This results in a transfer function relationship between motor angle and torque,

$$(sp^{-1}I + I - A^T K_c A K_m)\theta' = -A^T K_c A \gamma'. \quad (15)$$

E. Analyzing Actuator Passivity

This output mapped portion of the system will be passive if the integral of the work done on the environment by the output-mapped motor system is negative.

$$\int_0^T \gamma'^T(t) \dot{\theta}'(t) dt \leq 0 \quad (16)$$

A common frequency domain equivalent [23], [24] is that for all right half plane s , that is $s + \bar{s} > 0$,

$$H(s) + H^*(s) \leq 0, \quad (17)$$

for the transfer function $H(s) = \gamma'(s)/s\theta'(s)$.² We can express this transfer function

$$H(s) = -(A^T K_c A)^{-1}(p^{-1}I + I/s - A^T K_c A K_m/s) \quad (18)$$

and, since so much of this is symmetric, hardly anything is different in its conjugate transpose:

$$H^*(s) = -(p^{-1}I + I/\bar{s} - K_m A^T K_c A / \bar{s})(A^T K_c A)^{-1}. \quad (19)$$

Adding the two to form the matrix inequality in (17),

$$-2p^{-1}(A^T K_c A)^{-1} - \left(\frac{\bar{s} + s}{s\bar{s}} \right) ((A^T K_c A)^{-1} - K_m) \leq 0. \quad (20)$$

Note that, by the restriction on s , both $s + \bar{s} > 0$ and $s\bar{s} > 0$. The first term dominates as s approaches the $j\omega$ axis, and the second term dominates as $s \rightarrow 0^+$; both matrices

²The inequality is notation for negative semi-definiteness of the Hermitian matrix $H(s) + H^*(s)$.

must be negative semi definite to ensure passivity. Since these matrices are symmetric,

$$(A^T K_c A)^{-1} \geq 0 \iff K_c \geq 0, \quad (21)$$

$$R^T K_s R \geq K_d. \quad (22)$$

This is an upper bound on the desired stiffness matrix. The second condition is a lower bound:

$$(A^T K_c A)^{-1} - K_m \geq 0. \quad (23)$$

Substituting in our definitions of K_m and A , we can reduce this:

$$[R^T K_s R - K_d] \leq [R^T K_s R] \iff K_d \geq 0. \quad (24)$$

So, for passive controllers, the desired stiffness is bounded

$$0 \leq K_d \leq R^T K_s R. \quad (25)$$

This means that the pure desired stiffness of a series elastic driven system cannot exceed the passive stiffness of the system. A similar but restricted conclusion has been reached by researchers [25] [18] for the special case equivalent to $R^T K_s R$ diagonal. However, most tendon-routing strategies will lead to multi-articular joint stiffness (non-diagonal joint stiffness matrix) and thus instead of an element-wise comparison, we treat the above inequality as checking the positive definiteness of the following two matrix constructions,

$$R^T K_s R - K_d \geq 0 \quad (26)$$

$$K_d \geq 0 \quad (27)$$

F. Inclusion of Parallel Stiffness

Springs can also be added in parallel to the actuators in the form of torsional springs at the joints. If we define the parallel stiffness matrix as K_p , the analysis for passivity will change at Eq. (2) as,

$$\tau = R^T K_s R_m \theta' - (R^T K_s R + K_p) q \quad (28)$$

Hence, following the analysis, we will end up with new passivity conditions

$$R^T K_s R + K_p - K_d \geq 0 \quad (29)$$

$$K_d \geq K_p \quad (30)$$

Adding parallel compliance increases the maximum achievable desired controller stiffness without the need for stiffer series springs. However, adding parallel compliance also raises the lower bound on achievable desired stiffness. This makes intuitive sense as we would have to add feedforward compensation to overcome the torque due to the parallel compliance, i.e. inject more energy into the system.

G. Significance of Actuator Passivity

While a lack of passivity does not mean the overall system is necessarily unstable, it does mean that it could potentially add energy to the tendon-finger-environment system. For any particular type of non-passivity, there exists at least one frequency where a sinusoidal motor angle rate vector signal will produce a sinusoidal motor torque vector signal which, when the two signals are convolved, indicates adding positive energy to the tendon-hand-environment system. If the hand is designed such that this sinusoidal motor torque signal generates motion primarily in the same vector direction as the motor angle rate signal—exactly the case if each motor is paired with a unique joint—then vibrations in that linear subspace of motion gain energy proportional to the magnitude of the vibration. If the hand system also has damping, then the damping will remove some energy. This also scales with the amplitude of the oscillation. If the non-passive motor control adds more energy than the damping removes, then the system will vibrate out of control.

III. CASE STUDY : 2DOF TENDON-DRIVEN FINGER

A. System Model

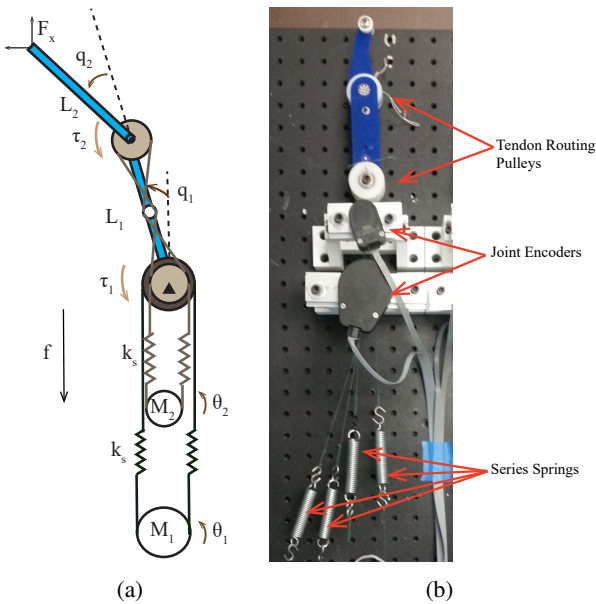


Fig. 1: a A 2-DOF tendon-driven planar robotic finger with tendon stiffness of k_s on all tendons. Two motors (M_1 and M_2) actuate the two DOFs using a belt-drive (2N) strategy. The tendons for the second joint route through an idler pulley on the first joint, resulting in compliant coupling between both joints. b Experimental equivalent 2-DOF testbed for validating the system analysis. The experimental system follows the same routing strategy as the simulation system

To validate our analysis of passivity boundaries, we model a planar, two DOF tendon-driven robotic finger (Fig.1),

$$I(q, \dot{q})\ddot{q} + C(q, \dot{q}) + B\dot{q} + K_p q = R^T f + J(q)^T F_{ext} \quad (31)$$

Based on the design, the dimension of the inertia matrix I is 2×2 , Coriolis and centripetal force matrix C is 2×1 and we can assume a small damping matrix B of dimension 2×2 . K_p is the parallel compliance matrix of size 2×2 .

The tendon force of the belt drive system ($f \in \mathbb{R}^{2 \times 1}$) can be estimated as

$$f = K_s(R_m\theta - Rq) \quad (32)$$

where R_m is the 2×2 diagonal transformation matrix of motor space to tendon space and R is a 2×2 transformation matrix for tendon space to joint space.

To emulate a joint stiffness (K_d) with its resting position at (q_d), the controller can be designed as,

$$\tau = K_d(q_d - q) \quad (33)$$

where $q_d = [q_{1,d}, q_{2,d}]^T$. In general practice, the controller stiffness matrix is chosen to be diagonal for independent control of the joints.

Now that a desired joint torque (τ) has been estimated, the actuator level controller has to calculate the displacement (θ_d) required to generate the desired torque.

$$\tau = R^T K_s(R_m\theta_d - Rq) \quad (34)$$

We exploit series compliance to generate forces indirectly via spring deflections, using position control at the actuator. In the simulation we make the simplifying assumption that the motor position controller parameters have been tuned such that all motor position dynamics have a first order response with a fixed rise time ($p = 1/t_r$).

$$\dot{\theta} = pI(\theta_d - \theta) \quad (35)$$

Using these equations, the motor displacement velocity which generates a desired joint torque is,

$$\dot{\theta} = pI(R_m^{-1}(K_s^{-1}R^{+T}\tau + Rq) - \theta) \quad (36)$$

where R^{+T} is the pseudo-inverse of the tendon routing map.

The series stiffness matrix (K_s) is diagonal with all springs of equal stiffness k_s . The tendon routing map R is based on the tendon topology chosen for fingers, and in general includes off-diagonal terms which lead to passive stiffness being coupled—that is, also having off-diagonal terms.

The effective passive joint stiffness system due to the series compliance (k_s)—the joint stiffness if the actuators are locked—can be represented as,

$$K_{j,passive} = R^T K_s R \quad (37)$$

In our case, the belt drive arrangement leads to the tendon routing map R

$$R = \begin{bmatrix} r_j & 0 \\ r_j & r_j \end{bmatrix} \quad (38)$$

where r_j is the radius of the circular pulleys at the joints.

Thus, the resultant passive joint stiffness matrix is,

$$K_{j,passive} = \begin{bmatrix} 4k_s r_j^2 & 2k_s r_j^2 \\ 2k_s r_j^2 & 2k_s r_j^2 \end{bmatrix} \quad (39)$$

Due to the routing strategy, the passive stiffness matrix is fully populated, with off-diagonal, multi-articular stiffness terms.

B. Experimental Setup

A 2-DOF tendon driven robotic finger testbed was designed (Fig. 1b) for validating the maximum achievable bound on joint stiffness. In order to allow the effects of passive stiffness to dominate over other parameters, the system was designed to keep friction and inertia as low as possible. Extension springs of equal stiffness were used as series compliance. Two rotary encoders were used to calculate the joint angles (U.S. Digital Inc.). Each DOF was actuated by one geared DC Motor (Maxon Motors Inc.) which was in turn controlled by a standalone closed loop position controller (Maxon EPOS controller). This allowed us to give desired position as the input to the actuator system. All of the controllers were written in Labview and executed by an FPGA based embedded controller (National Instruments CompactRIO). All high level controllers were running at 2KHz while all data acquisition was running at 40KHz. For validation, we used series springs of varying stiffnesses, but for the sake of space, we will show just the results with $k_s = 1873$ N/m. The joint pulleys were chosen with equal diameters $r_j = 18.875$ mm.

IV. VALIDATION

To validate the maximum achievable stability bounds, we tested the impulse response of the robotic finger at different desired joint stiffnesses. We will discuss three interesting stiffness boundary behaviors which we encountered (Fig. 2). Due to the symmetric nature of the passive and desired stiffness matrices, they can be represented as ellipsoids in joint stiffness space. We overlaid the ellipsoids on top of each other to gain an intuitive understanding of the interaction of the desired stiffness and passive stiffness matrices.

The first column of the results (Fig. 2 a, d and g) shows a stable isotropic desired stiffness matrix with each joint set to a stiffness of 0.5 N-m/rad. This value satisfies the passivity conditions derived in Eq. (26) and (27). The impulse response was stable as expected. The simulation d oscillates much more than the experimental system g due to unmodeled friction in the experimental system. All values of K_d smaller than this value were stable to impulses as well. However, when the isotropic stiffness becomes larger than 0.50 N-m/rad, the simulation system became unstable, as predicted by Eq. 25.

The second column (Fig. 2 b, e and h) is an unstable case where we chose a diagonal desired stiffness matrix with the stiffness at joint 1 as 0.9 N-m/rad and stiffness at joint 2 as 0.5 N-m/rad. The passivity bounds fail for this case and the results in both the simulation and experiments reflect that. Note that the unstable vibrations in the experimental space appear saturated due to a safety measure implemented into the position controller which limits the maximum displacement of the actuator.

In the third column (Fig. 2 c, f and i), we chose the desired stiffness as a scaled value of the passive joint stiffness matrix including multi-articular terms. It is interesting to note that the system remained stable at a desired joint 1 stiffness of 2 N-m/rad and joint 2 and multiarticular stiffness of 1 N-m/rad, which are much higher values than the previous cases that contained only diagonal terms. It makes intuitive sense when we look at the graphical representation of these stiffnesses. When the eigenvectors of the desired stiffness matrix and passive stiffness matrix are the same, the stability criteria just reduces to an element-wise difference of the (uniquely ordered) eigenvalues of the passive stiffness matrix and desired stiffness matrix.

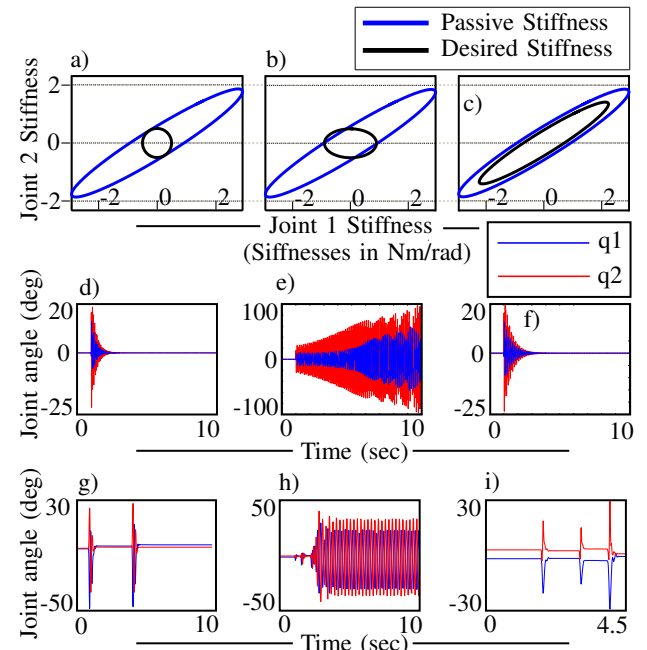


Fig. 2: Impact stability of the system. a, b and c show the graphical representation of the stiffness ellipse (torques from any unit displacement vector) due to passive elements in blue and the desired stiffness in black. Where b shows the instability criteria and c shows that much higher stiffnesses can be achieved through control if multiarticular stiffness terms are included in the desired stiffness matrix. d, e and f show the simulations and g, h and i show experimental results of impulse responses. The blue line is joint 1 and red line is joint 2 angle.

V. CONCLUSION AND DISCUSSION

In this study, we have for the first time derived, using a passivity-based approach, the maximum achievable limits on joint stiffness controllers for robotic fingers with compliant coupling between the joints. We found that the maximum stiffness achievable is bounded by the passive stiffness of the system. We validated this by choosing a test case of a 2 DOF tendon driven robotic finger with multi-articular passive

stiffness. The impulse response characteristics showed an agreement with our theoretical stiffness boundaries.

The analysis of passivity provides an insight into a mechanical design paradigm. On analyzing the upper bound inequality, we can see that design parameters such as the tendon routing pulley radii can be used to modify the stability boundaries. The shape of the passive stiffness ellipse can be modified by having pulleys of different radii at every joint. However, size constraints and the torque requirement at the joints put limits on the selection of pulley radii.

Another approach to increasing stiffness boundaries would be to increase the stiffness of the series springs. However, as the inertia of the finger joints are low, a higher series stiffness will raise the natural frequency of the joint. This might lead to unfavorable noise transmission from the actuators to the joint and vice-versa, both of which might be damaging to the system in case of impacts and undesirable for robust manipulation. Series springs are usually chosen based on an estimate of the maximum expected torque that needs to be generated at the joints as well as for safe environmental interaction. A very stiff transmission might be able to generate larger forces, but it also loses the key features of passive compliance.

We showed in theory that adding stiffness in parallel to the actuators was a viable alternative to increasing series stiffness for larger stability boundaries. Well-chosen parallel compliance can also be used to boost the performance of specific joints depending on the task, giving the designer the ability to customize the intrinsic properties of the fingers if the task is known. However, the lower bound inequality showed that adding parallel compliance and desiring a very low desired stiffness can cause non-passive controller behavior which might lead to instability.

Impulse response experiments showed that damping/friction also increases the achievable stiffness boundaries of the system above the theoretical limit of passive stiffness. However, miniature linear dampers are extremely difficult to manufacture and have non-linearities such as stiction and hysteresis. Friction is undesirable for fine end-tip force control which is a key requirement for manipulation.

REFERENCES

- [1] A. Bicchi, "Hands for dexterous manipulation and robust grasping: A difficult road toward simplicity," *IEEE Transactions on Robotics and Automation*, vol. 16, pp. 652–662, 2000.
- [2] X. H. Gao, M. H. Jin, L. Jiang, Z. W. Xie, P. He, L. Yang, Y. W. Liu, R. Wei, H. G. Cai, and H. Liu, "The hit/dlr dexterous hand: Work in progress," in *IEEE International Conference on Robotics and Automation*, vol. 3, 2003, pp. 3164–3168.
- [3] M. Grebenstein, M. Chalon, W. Friedl, S. Haddadin, T. Wimböck, G. Hirzinger, and R. Siegwart, "The hand of the dlr hand arm system: Designed for interaction," *The International Journal of Robotics Research*, vol. 31, no. 13, pp. 1531–1555, 2012.
- [4] L. Bridgwater, C. Ihrke, M. Diftler, M. Abdallah, N. Radford, J. Rogers, S. Yayathi, R. Askew, D. Linn, and G. Motors, "The robonaut 2 hand—designed to do work with tools," in *IEEE International Conference on Robotics and Automation*, 2012.
- [5] A. Dollar and R. Howe, "The highly adaptive SDM hand: Design and performance evaluation," *The International Journal of Robotics Research*, vol. 29, no. 5, p. 585, 2010.
- [6] N. Hogan, "Impedance control: An approach to manipulation," *Journal of Dynamic Systems, Measurement, and Control*, vol. 107, pp. 1–24, 1985.
- [7] M. Abdallah, R. Platt, C. Wampler, and B. Hargrave, "Applied joint-space torque and stiffness control of tendon-driven fingers," in *IEEE-RAS International Conference on Humanoid Robots (Humanoids)*, 2010, pp. 74–79.
- [8] T. Lan, Y. W. Liu, M. H. Jin, S. W. Fan, H. G. Fang, J. J. Xia, and H. Liu, "DSP & FPGA-based joint impedance controller for DLR/HIT II dexterous robot hand," in *IEEE/ASME International Conference on Advanced Intelligent Mechatronics*, 2009.
- [9] G. Pratt and M. Williamson, "Series elastic actuators," in *IEEE/ASME International Conference of Intelligent Robots and Systems (IROS)*, vol. 1, 1995, pp. 399–406.
- [10] R. Filippini, S. Sen, and A. Bicchi, "Toward soft robots you can depend on," in *IEEE Robotics & Automation Magazine*, 2008.
- [11] B. Vanderborght, A. Albu-Schaeffer, A. Bicchi, E. Burdet, D. Caldwell, R. Carloni, M. Catalano, O. Eiberger, W. Friedl, G. Ganesh, M. Garabini, M. Grebenstein, G. Grioli, S. Haddadin, H. Hoppner, A. Jafari, M. Lafranchi, D. Lefebvre, F. Petit, S. Stramigioli, N. Tsagarakis, M. Van Damme, R. Van Ham, L. Visser, and Wol, "Variable impedance actuators: a review," *Robotics and Autonomous Systems*, 2013.
- [12] M. Grebenstein, A. Albu-Schaffer, T. Bahls, M. Chalon, O. Eiberger, W. Friedl, R. Gruber, S. Haddadin, U. Hagn, R. Haslinger, et al., "The DLR hand arm system," in *IEEE International Conference on Robotics and Automation (ICRA)*, 2011, pp. 3175–3182.
- [13] M. A. Diftler, J. S. Mehling, M. E. Abdallah, N. A. Radford, L. B. Bridgwater, A. M. Sanders, R. S. Askew, D. M. Linn, J. D. Yamokoski, and F. A. Permenter, "Robonaut 2 - the first humanoid robot in space," in *IEEE International Conference on Robotics and Automation (ICRA)*, 2011, pp. 2178–2183.
- [14] P. Rao, T. D. Niehues, and A. D. Deshpande, "Effect of parallel compliance on stability of robotic hands with series elastic actuators," in *ASME 2015 Dynamic Systems and Controls Conference, Columbus, Ohio*. ASME International, Oct 2015. [Online]. Available: <http://dx.doi.org/10.1115/DSCC2015-9917>
- [15] M. Grimmer, M. Eslamy, S. Gliech, and A. Seyfarth, "A comparison of parallel-and series elastic elements in an actuator for mimicking human ankle joint in walking and running," in *IEEE International Conference on Robotics and Automation (ICRA)*, 2012, pp. 2463–2470.
- [16] F. Lotti, P. Tiezzi, G. Vassura, L. Biagiotti, G. Palli, and C. Melchiorri, "Development of UB hand 3: Early results," in *IEEE International Conference on Robotics and Automation (ICRA)*, 2005, pp. 4488–4493.
- [17] T. Niehues, P. Rao, and A. Deshpande, "Compliance in parallel to actuators for improving stability of robotic hands during grasping and manipulation," *International Journal of Robotics Research*, 2014.
- [18] H. Vallery, J. Veneman, E. Van Asseldonk, R. Ekkelenkamp, M. Buss, and H. Van Der Kooij, "Compliant actuation of rehabilitation robots," *IEEE Robotics & Automation Magazine*, vol. 15, no. 3, pp. 60–69, 2008.
- [19] A. Albu-Schaffer, M. Fischer, G. Schreiber, F. Schoeppe, and G. Hirzinger, "Soft robotics: what cartesian stiffness can obtain with passively compliant, uncoupled joints?" in *Intelligent Robots and Systems, 2004. (IROS 2004). Proceedings. 2004 IEEE/RSJ International Conference on*, vol. 4, Sept 2004, pp. 3295–3301 vol.4.
- [20] A. Ajoudani, N. Tsagarakis, and A. Bicchi, "On the role of robot configuration in cartesian stiffness control," in *Robotics and Automation (ICRA), 2015 IEEE International Conference on*, May 2015, pp. 1010–1016.
- [21] N. Hogan, "Adaptive control of mechanical impedance by coactivation of antagonist muscles," *IEEE Transactions on Automatic Control*, vol. 29, no. 8, pp. 681–690, 1984.
- [22] H. Kobayashi, K. Hyodo, and D. Ogane, "On tendon-driven robotic mechanisms with redundant tendons," *The International Journal of Robotics Research*, vol. 17, no. 5, pp. 561–571, 1998.
- [23] S. P. Boyd, L. El Ghaoui, E. Feron, and V. Balakrishnan, *Linear Matrix Inequalities in System and Control Theory*. SIAM, 1994, vol. 15.
- [24] M. Green and D. J. N. Limebeer, *Linear Robust Control*. Prentice Hall, 1995.
- [25] H. Mehdi and O. Boubaker, "Stiffness and impedance control using lyapunov theory for robot-aided rehabilitation," *International Journal of Social Robotics*, vol. 4, no. 1, pp. 107–119, 2012. [Online]. Available: <http://dx.doi.org/10.1007/s12369-011-0128-5>